AD-A098 940 ROME AIR DEVELOPMENT CENTER GRIFFISS AFB NY F/G 20/14
THE REFLECTION PROPERTIES OF CONDUCTING SLABS.(U)
JAN 81 P A KOSSEY, E A LEWIS
UNCLASSIFIED RADC-TR-80-371 NL

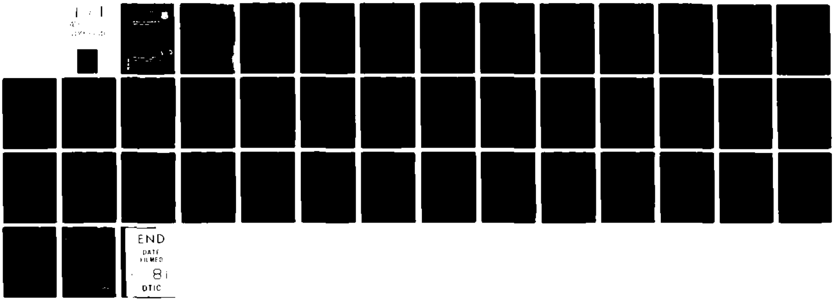

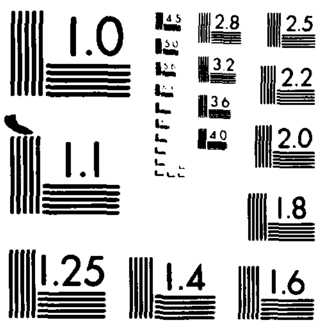

MICROCOPY RESOLUTION TEST CHART
NATIONAL BUREAU OF STANDARDS 1963 A

LEVEL

AD A098940

THE REFLECTION PROPERTIES OF CONDUCTING SLABS

[illegible]

[illegible] A. Lewis

APPROVED FOR PUBLIC RELEASE; DISTRIBUTION UNLIMITED

This report has been reviewed by the RADC Public Affairs Office [illegible] releasable to the National Technical Information Service (NTIS). [illegible] will be releasable to the general public, including foreign nations.

RADC-TR-80-371 has been reviewed and is approved for publication.

APPROVED: Terence J. Elkins

TERENCE J. ELKINS
Chief, Propagation Branch
Electromagnetic Sciences Division

APPROVED: Allan C. Schell

ALLAN C. SCHELL
Chief, Electromagnetic Sciences Division

FOR THE COMMANDER: John P. Huss

JOHN P. HUSS
Acting Chief, Plans Office

If your address has changed or if you wish to be removed from [illegible] ing list, or if the addressee is no longer employed by your [illegible] please notify RADC (EEP), Hanscom AFB MA 01731. This will [illegible] taining a current mailing list.

Do not return this copy. Retain or destroy.

Unclassified

SECURITY CLASSIFICATION OF THIS PAGE (When Data Entered)

REPORT DOCUMENTATION PAGE		READ INSTRUCTIONS BEFORE COMPLETING FORM
1. REPORT NUMBER RADC-TR-80-371 ✓	2. GOVT ACCESSION NO. AD-A098940	3. RECIPIENT'S CATALOG NUMBER
4. TITLE (and Subtitle) THE REFLECTION PROPERTIES OF CONDUCTING SLABS.		5. TYPE OF REPORT & PERIOD COVERED In-House
		6. PERFORMING ORG. REPORT NUMBER
7. AUTHOR(s) Paul A. Kossey, Edward A. Lewis		8. CONTRACT OR GRANT NUMBER(s)
9. PERFORMING ORGANIZATION NAME AND ADDRESS Deputy for Electronic Technology (RADC/EEP) Hanscom AFB Massachusetts 01731		10. PROGRAM ELEMENT PROJECT, TASK AREA & WORK UNIT NUMBERS 61102F 2305J201
11. CONTROLLING OFFICE NAME AND ADDRESS Deputy for Electronic Technology (RADC/EEP) Hanscom AFB Massachusetts 01731		12. REPORT DATE January 1981
		13. NUMBER OF PAGES 42
14. MONITORING AGENCY NAME & ADDRESS(if different from Controlling Office)		15. SECURITY CLASS. (of this report) Unclassified
		15a. DECLASSIFICATION DOWNGRADING SCHEDULE

16. DISTRIBUTION STATEMENT (of this Report)

Approved for public release; distribution unlimited.

17. DISTRIBUTION STATEMENT (of the abstract entered in Block 20, if different from Report)

18. SUPPLEMENTARY NOTES

19. KEY WORDS (Continue on reverse side if necessary and identify by block number)

Lower ionosphere
C-layer
Ionospheric reflectivity

20. ABSTRACT (Continue on reverse side if necessary and identify by block number)

The exact monochromatic solution for the plane wave reflection by a flat homogeneous slab of arbitrary thickness and conductivity is written for both transverse magnetic (TM) and transverse electric (TE) polarizations. The reflected waveforms for an incident impulse and for a low frequency pulse are then written as Fourier integrals and are numerically solved for a number of special cases of interest for application to studies of the reflection properties and nature of the lowest regions of the daytime ionosphere.

DD FORM 1 JAN 73 1473 EDITION OF 1 NOV 65 IS OBSOLETE

Unclassified

SECURITY CLASSIFICATION OF THIS PAGE (When Data Entered)

Preface

The authors gratefully acknowledge the enlightening conversations with Mr. Edward Cohen of Arcon Corporation, Waltham, Massachusetts, concerning the numerical integration techniques used to generate results described in this report. Appreciation is also extended to Mr. Wayne I. Klemetti of the Propagation Branch, Rome Air Development Center, for his aid in preparing the graphics shown throughout the report.

Contents

Contents

Illustrations

The Reflection Properties of Conducting Slabs

1. INTRODUCTION

Low frequency pulse ionospheric reflection data recently described by Rasmussen et al[1] indicate that the daytime lower ionosphere sometimes has a weak reflecting layer below the solar zenith angle controlled D-region, at an altitude at which electron-neutral collisions dominate over geomagnetic field effects. The electromagnetic effect of such a layer is essentially that of an isotropic faintly conducting one. Attempts to reconstruct the properties of such layers from the pulse reflection waveforms led the authors to consider the reflection properties of an idealized slab of uniform conductivity and finite thickness. The results of these studies are described in this report. A somewhat analogous study for the case of reflections from a lossless dielectric slab already appears in the recent literature.[2]

Received for publication 5 January 1981

1. Rasmussen, J.E., Kossey, P.A., and Lewis, E.A. (1980) Evidence of an ionospheric reflecting layer below the classical D region, J. Geophys. Res. 85:3037.
2. Tabbara, W. (1979) Reconstruction of permittivity profiles from a spectral analysis of the reflection coefficient, IEEE Trans. on Antennas and Prop. AP-27:241.

2. THE PLANE WAVE REFLECTION COEFFICIENTS OF CONDUCTING SLABS

2.1 The General Problem and Pertinent Definitions

The reflection problem under consideration is illustrated in Figure 1, where a plane wave of unit amplitude and frequency $\underline{w}$ is obliquely incident on a conducting slab of finite thickness, $\underline{h}$. The electromagnetic properties of the slab are characterized by a conductivity $\underline{\sigma}$, a propagation constant $\underline{k}$, a dielectric constant $\underline{\epsilon}$, and a permeability $\underline{\mu_o}$. It is further assumed that the slab is immersed in free space which has a dielectric constant $\epsilon_o = 8.854 \times 10^{-12}$ F/m, a permeability $\mu_o = 4\pi \times 10^{-7}$ H/m, and a propagation constant k_o. In general there will be a reflected wave in the space below the slab, and a transmitted wave in the space above the slab. The ratio of the reflected and incident plane waves, measured at the same point, is defined as the reflection coefficient of the slab, R. In the notation of Figure 1, $R = \overline{F2}/\overline{F1}$. Similarly, a transmission coefficient, T, can be defined as the ratio $\overline{F3}/\overline{F1}$ at some specified point in space. The main purpose of this section is to determine the reflection coefficients for conducting slabs of arbitrary thickness and conductivity.

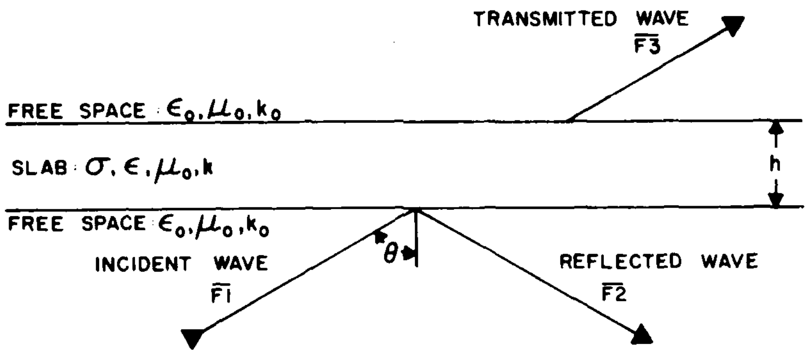

Figure 1. Plane Waves Reflected and Transmitted by a Conducting Slab

In what follows it is assumed that the incident plane wave is travelling upwards, in general obliquely, and the direction of the X-axis is chosen so that the wave normal is in the X-Z plane and is pointing in the positive directions of both X and Z, at an angle θ to the Z-axis. Then the X-Z plane is called the "plane-of-incidence," and two plane wave reflection coefficients can be defined. For the case when the plane wave has its magnetic field transverse to the plane-of-incidence, the reflection coefficient will be termed TM- and will be denoted R_{TM}.

Alternately, for the case when the plane wave has its electric field transverse to the plane-of-incidence, the reflection coefficients will be termed TE-, and will be denoted by R_{TE}.

2.2 TM-Reflection Coefficients

2.2.1 EQUATIONS FOR AN INCIDENT TM-WAVE

The geometry for the case of an obliquely incident plane TM-wave, in free space, is illustrated in Figure 2. The magnetic field component of the incident wave is solely in the direction of the Y-axis and, under the assumption that it is of unit amplitude, it can be expressed simply as

$$H_y = e^{ik_o \overline{MP} - iwt} ,$$

where MP represents the down-wave distance, which can be expressed as $x \sin\theta + z \cos\theta$, from the geometry shown in Figure 2. Since the whole wave pattern must vary as $e^{ik_o x \sin\theta - iwt}$, this factor will be supressed in the development that follows.

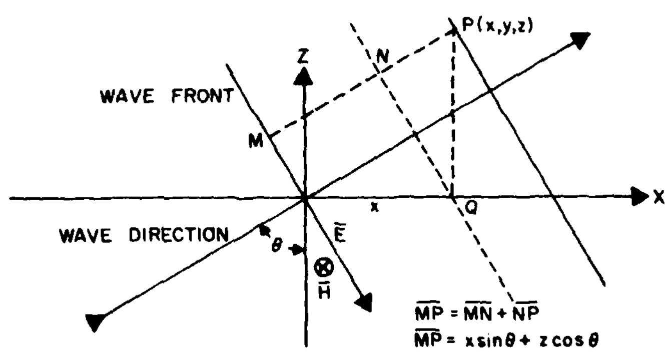

Figure 2. Obliquely Incident TM-Waves on a Cartesian Coordinate System

Using familiar free-space plane wave concepts, the components of the incident plane wave are

$$H_y = e^{ik_o z \cos\theta} , \tag{1}$$

$$E_x = Z_o \cos\theta \, e^{ik_o z \cos\theta} , \tag{2}$$

and

$$E_z = -Z_o \sin\theta \, e^{ik_o z \cos\theta} \tag{3}$$

where $Z_o = (\mu_o/\epsilon_o)^{1/2} = k_o/\epsilon_o w$, and $k_o = w/c$ ($c = 3 \times 10^8$ m/sec).

2.2.2 EQUATIONS FOR THE TRANSMITTED TM-WAVE

The transmitted wave (see Figure 1) has a form similar to the incident wave. Assuming the amplitude of the transmitted wave to be T, its components are

$$H_y = T e^{ik_o z \cos\theta} , \tag{4}$$

$$E_x = Z_o T \cos\theta \, e^{ik_o z \cos\theta} , \tag{5}$$

and

$$E_z = -Z_o T \sin\theta \, e^{ik_o z \cos\theta} . \tag{6}$$

2.2.3 EQUATIONS FOR THE REFLECTED TM-WAVE

Let the amplitude of the reflected wave be R_{TM}. This wave is similar in form to the incident and transmitted waves except for (a) its amplitude R_{TM}, (b) its downward direction of travel, and (c) its E_x field component, which is negative. Thus, for the reflected wave,

$$H_y = R_{TM} e^{ik_o z \cos\theta} , \tag{7}$$

$$E_x = -R_{TM} Z_o \cos\theta \, e^{-ik_o z \cos\theta} , \tag{8}$$

and

$$E_z = -R_{TM} Z_o \sin\theta \, e^{-ik_o z \cos\theta} . \tag{9}$$

2.2.4 EQUATIONS FOR THE WAVES INSIDE THE SLAB

Since the plane wave solutions for the waves inside of the conducting slab are more complicated and less familiar than the free-space ones, they will be developed here from first principles, using a consistent notation. In doing this the following assumptions are made:

(a) H_y, E_x, and E_z are the only field components,

(b) none of the field components vary with y,

(c) the suppressed factor is $e^{ik_o x \sin\theta - iwt}$,

(d) the operator $\partial/\partial x$ is equivalent to multiplier $ik_o \sin\theta$, and

(e) the operator $\partial/\partial t$ is equivalent to the multiplier $-iw$.

Under these assumptions the pertinent Maxwell's equations are

$$\text{curl}\,\overline{E} = -\mu_o\,\partial\overline{H}/\partial t = iw\mu_o\overline{H} \quad ,$$

which can be written

$$\begin{vmatrix} \overline{x}_o & \overline{y}_o & \overline{z}_o \\ \partial/\partial x & 0 & \partial/\partial z \\ E_x & 0 & E_z \end{vmatrix} = i\mu_o w H_y \overline{y}_o \quad , \tag{10}$$

and

$$\text{curl}\,\overline{H} = \overline{E}\sigma + \epsilon_o\,\partial\overline{E}/\partial t = \overline{E}\sigma - iw\epsilon_o\overline{E}$$

$$= -iw\epsilon\overline{E} \quad ,$$

where

$$\epsilon = \epsilon_o(1 + i\sigma/w\epsilon_o) \quad ,$$

which can be written

$$\begin{vmatrix} \overline{x}_o & \overline{y}_o & \overline{z}_o \\ \partial/\partial x & 0 & \partial/\partial z \\ 0 & H_y & 0 \end{vmatrix} = -iw\epsilon\overline{E} \quad . \tag{11}$$

Carrying out the operations shown in Eqs. (10) and (11) yield

$$\frac{\partial E_x}{\partial z} - \frac{\partial E_z}{\partial x} \quad i\mu_o w H_y \quad , \tag{12}$$

$$\frac{\partial H_y}{\partial z} = i w \epsilon E_x \quad , \tag{13}$$

and

$$\frac{\partial H_y}{\partial x} = - i w \epsilon E_z \quad . \tag{14}$$

Using the operator $\partial/\partial x$ and then consolidating these equations gives

$$\frac{\partial E_x}{\partial z} = i k_o \sin\theta \; E_z + i \mu_o w H_y \quad , \tag{15}$$

$$\frac{\partial H_y}{\partial z} = i w \epsilon E_x \quad , \tag{16}$$

and

$$k_o \sin\theta \; H_y = - w \epsilon E_z \quad . \tag{17}$$

It can be shown that these equations are satisfied by a plane wave of the form

$$H_y = e^{ikz \cos\theta} \quad , \tag{18}$$

$$E_z = - \frac{k_o \sin\theta}{\epsilon w} e^{ikz \cos\theta} \quad , \tag{19}$$

and

$$E_x = \frac{k \cos\theta}{\epsilon w} e^{ikz \cos\theta} \quad , \tag{20}$$

provided

$$\cos\theta \; k = \pm \sqrt{\epsilon \mu_o w^2 - k_o^2 \sin^2\theta} \quad , \tag{21}$$

or, after rearranging,

$$k = \pm k_o \sqrt{1 + i \frac{\sigma}{w\epsilon_o \cos^2 \theta}} \ . \tag{22}$$

If both the real and imaginary parts of k are positive, the wave is an upward going one with decreasing amplitude, while if both the real and imaginary parts of k are negative, the wave is a downward going one with decreasing amplitude. In the development which follows only the positive root will be taken since the negative sign for the downgoing waves can be appropriately incorporated into the equations.

Generally there are both upgoing and downgoing waves inside the slab. Letting their amplitudes be U and D respectively, the following equations apply:

<u>Upgoing</u>

$$H_y = U e^{ikz \cos \theta} \ , \tag{23}$$

$$E_z = \frac{-U k_o \sin \theta}{\epsilon w} e^{ikz \cos \theta} \ , \tag{24}$$

and

$$E_x = \frac{U k \cos \theta}{\epsilon w} e^{ikz \cos \theta} \ ; \tag{25}$$

<u>Downgoing</u>

$$H_y = D e^{-ikz \cos \theta} \ , \tag{26}$$

$$E_z = \frac{-D k_o \sin \theta}{\epsilon w} e^{-ikz \cos \theta} \ , \tag{27}$$

and

$$E_x = \frac{-D k \cos \theta}{\epsilon w} e^{-ikz \cos \theta} \ . \tag{28}$$

2.2.5 BOUNDARY CONDITIONS

The appropriate boundary conditions are that at the two boundaries of the slab, the tangential $\overline{H}$ and $\overline{E}$ fields must be continuous. At the lower boundary

(that is, at $z = 0$) the condition than tangential $\overline{H}$ is continuous gives, from Eqs. (1), (7), (23), and (26),

$$1 + R_{TM} = U + D \quad . \tag{29}$$

Similarly, the condition that tangential $\overline{E}$ is continuous yields, from Eqs. (2), (8), (25), and (28),

$$Z_o \cos\theta (1 - R_{TM}) = \frac{k \cos\theta}{\epsilon w} (U - D) \quad . \tag{30}$$

At the upper boundary of the slab, $z = h$, the respective boundary conditions require, from Eqs. (4), (23), and (26), and Eqs. (5), (25), and (28),

$$U\, e^{ikh\cos\theta} + D\, e^{-ikh\cos\theta} = T\, e^{ik_o h\cos\theta} \quad , \tag{31}$$

and

$$\frac{k\cos\theta}{\epsilon w}\left[U\, e^{ikh\cos\theta} - D\, e^{-ikh\cos\theta}\right] = T\, \frac{k_o \cos\theta}{\epsilon_o w}\, e^{ik_o h\cos\theta} \quad . \tag{32}$$

2.2.6 SOLUTION OF THE EQUATIONS TO OBTAIN THE TM-REFLECTION COEFFICIENT

Equations (29), (30), (31), and (32) permit solutions for the four unknowns, R_{TM}, T, U, and D. The solution for the TM-reflection coefficient of the slab is outlined below.

After removing common factors and denominators, the pertinent equations can be written as

$$1 + R_{TM} = U + D \quad , \tag{33}$$

$$(1 - R_{TM})\, k_o \epsilon = k \epsilon_o (U - D) \quad , \tag{34}$$

$$U\, e^{ikh\cos\theta} + D\, e^{-ikh\cos\theta} = T\, e^{ik_o h\cos\theta} \quad , \tag{35}$$

and

$$(U\, e^{ikh\cos\theta} - D\, e^{ikh\cos\theta})\, k\epsilon_o = k_o \epsilon\, T\, e^{ik_o h\cos\theta} \quad . \tag{36}$$

Equations (35) and (36) can be combined to eliminate the factor T yielding

$$U(k_o\epsilon - k\epsilon_o)\, e^{ikh\cos\theta} = -D(k\epsilon_o + k_o\epsilon)\, e^{-ikh\cos\theta} \quad ,$$

or

$$D = -Q\,U\, e^{i2kh\cos\theta} \quad , \tag{37}$$

where

$$Q \equiv \frac{k_o\epsilon - k\epsilon_o}{k_o\epsilon + k\epsilon_o}$$

$$= \frac{\left(1 + \frac{i\sigma}{w\epsilon_o}\right) - \left(1 + \frac{i\sigma}{w\epsilon_o \cos^2\theta}\right)^{1/2}}{\left(1 + \frac{i\sigma}{w\epsilon_o}\right) + \left(1 + \frac{i\sigma}{w\epsilon_o \cos^2\theta}\right)^{1/2}} \quad . \tag{38}$$

After insertion of the expression for D given by Eq. (37) into Eqs. (33) and (34), they can be combined to eliminate U, leaving

$$(1 - R_{TM})k_o\epsilon(1 + Q\, e^{i2kh\cos\theta}) = (1 + R_{TM})k\epsilon_o(1 - Q\, e^{i2kh\cos\theta}) \quad . \tag{39}$$

Finally, Eq. (39) can be solved to find the slab reflection coefficient

$$R_{TM} = \frac{Q(1 - e^{i2kh\cos\theta})}{(1 - Q^2\, e^{i2kh\cos\theta})} \quad . \tag{40}$$

2.3 TE-Reflection Coefficients

2.3.1 EQUATIONS FOR AN INCIDENT TE-WAVE

The geometry for the case of an obliquely incident plane TE-wave in free space is illustrated in Figure 3. The nonzero components of the wave are now E_y, H_z, and H_z, and the forms of the incident, transmitted, and reflected waves can be written from a knowledge of the plane wave free-space solutions. As before, the factor $e^{ik_o x\sin\theta - iwt}$ will be suppressed in the development that follows. Assuming that the incident wave is of unit amplitude, its components are

$$E_y = e^{ik_o z \cos\theta} \quad , \tag{41}$$

$$H_x = -(1/Z_o) \cos\theta \, e^{ik_o z \cos\theta} \quad . \tag{42}$$

and

$$H_z = (1/Z_o) \sin\theta \, e^{ik_o z \cos\theta} \quad . \tag{43}$$

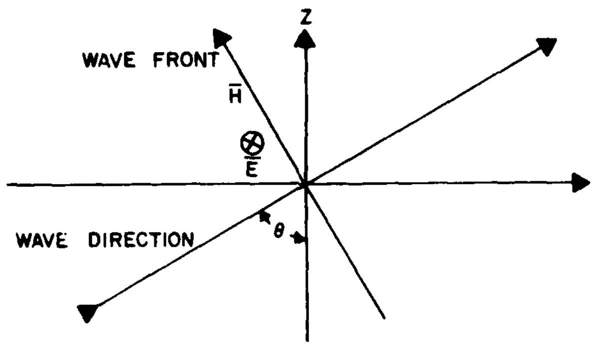

Figure 3. Obliquely Incident TE-Waves on a *Cartesian Coordinate System*

2.3.2 EQUATIONS FOR THE TRANSMITTED TE-WAVE

The transmitted wave has the same form as the incident plane wave, but with an amplitude T. Thus

$$E_y = T \, e^{ik_o z \cos\theta} \quad , \tag{44}$$

$$H_x = -(T/Z_o) \cos\theta \, e^{ik_o z \cos\theta} \quad , \tag{45}$$

and

$$H_z = (T/Z_o) \sin\theta \, e^{ik_o z \cos\theta} \quad . \tag{46}$$

2.3.3 EQUATIONS FOR THE REFLECTED TE-WAVE

The reflected wave is similar in form to the incident wave but differs from it by (a) its amplitude R_{TE}, (b) its downward direction of travel, and (c) its H_x component, which is negative. Thus,

$$E_y = R_{TE}\, e^{-ik_o z \cos\theta} \quad , \tag{47}$$

$$H_x = (R_{TM}/Z_o) \cos\theta\, e^{-ik_o z \cos\theta} \quad , \tag{48}$$

and

$$H_z = (R_{TM}/Z_o) \sin\theta\, e^{-ik_o z \cos\theta} \quad . \tag{49}$$

2.3.4 EQUATIONS FOR THE WAVES INSIDE THE SLAB

Since only E_y, H_x, and H_z exist, and since these are not functions of y, the Maxwell equation curl $\overline{E} = iw\mu_o \overline{H}$ may be written

$$\begin{vmatrix} \overline{x}_o & \overline{y}_o & \overline{z}_o \\ \partial/\partial x & 0 & \partial/\partial z \\ 0 & E_y & 0 \end{vmatrix} = iw\mu_o (H_x \overline{x}_o + H_z \overline{z}_o) \quad .$$

Since the operation $\partial/\partial x$ is equivalent to multiplying by $ik_o \sin\theta$, this reduces to two equations,

$$-\frac{\partial E_y}{\partial z} = iw\mu_o H_x \quad , \tag{50}$$

and

$$k_o \sin\theta\, E_y = w\mu_o H_z \quad . \tag{51}$$

Similarly the Maxwell equation curl $\overline{H} = -iw\epsilon\overline{E}$ can be written

$$\begin{vmatrix} \overline{x}_o & \overline{y}_o & \overline{z}_o \\ \partial/\partial x & 0 & \partial/\partial z \\ H_x & 0 & H_z \end{vmatrix} = -iw\epsilon E_y \overline{y}_o \quad ,$$

which reduces to

$$ik_o \sin\theta\, H_z - (\partial H_x/\partial z) = iw\epsilon E_y \quad . \tag{52}$$

It can be readily verified that Eqs. (50), (51), and (52) are satisfied by plane waves of the form

$$E_y = e^{ikz\cos\theta} \quad , \tag{53}$$

$$H_x = -\frac{k\cos\theta}{w\mu_o} e^{ikz\cos\theta} \quad , \tag{54}$$

and

$$H_z = \frac{k_o \sin\theta}{w\mu_o} e^{ikz\cos\theta} \quad , \tag{55}$$

where k has the same value as given in the TM-case by Eq. (22). As discussed previously the positive root for k will be taken since the appropriate signs for the upgoing and downgoing waves can be easily incorporated into the equations. Letting the amplitudes of the upgoing and downgoing waves inside the slab be U and D respectively, the following equations apply:

Upgoing

$$E_y = U\, e^{ikz\cos\theta} \quad , \tag{56}$$

$$H_x = -\frac{U\, k\cos\theta}{w\mu_o} e^{ikz\cos\theta} \quad , \tag{57}$$

and

$$H_z = \frac{U\, k_o \sin\theta}{w\mu_o} e^{ikz\cos\theta} \quad ; \tag{58}$$

Downgoing

$$E_y = D\, e^{-ikz\cos\theta} \quad , \tag{59}$$

$$H_x = \frac{D\,k\cos\theta}{w\mu_0}\,e^{-ikz\cos\theta} \quad , \tag{60}$$

and

$$H_z = \frac{D\,k_0\sin\theta}{w\mu_0}\,e^{-ikz\cos\theta} \quad . \tag{61}$$

2.3.5 BOUNDARY CONDITIONS

As given earlier, the boundary conditions are that at the two boundaries of the slab, the tangential $\overline{E}$ and $\overline{H}$ fields must be continuous. At the lower boundary, at $z = 0$, the condition that tangential $\overline{E}$ is continuous gives, from Eqs. (41), (47), (56), and (59),

$$1 + R_{TE} = U + D \quad . \tag{62}$$

Similarly, the condition that tangential $\overline{H}$ is continuous yields, from Eqs. (42), (48), (57), and (60),

$$-\frac{\cos\theta}{Z_0} + \frac{R_{TE}\cos\theta}{Z_0} = -\frac{U\,k\cos\theta}{w\mu_0} + \frac{D\,k\cos\theta}{w\mu_0} \quad . \tag{63}$$

At the upper boundary of the slab, $z = h$, the respective boundary conditions require, from Eqs. (44), (56), and (59), and Eqs. (45), (57), and (60),

$$U\,e^{ikh\cos\theta} + D\,e^{-ikh\cos\theta} = T\,e^{ik_0 h\cos\theta} \quad , \tag{64}$$

and

$$-\frac{U\,k\cos\theta}{w\mu_0}\,e^{ikh\cos\theta} + \frac{D\,k\cos\theta}{w\mu_0}\,e^{-ikh\cos\theta} = -\frac{T\cos\theta}{Z_0}\,e^{ik_0 h\cos\theta} \quad . \tag{65}$$

After removal of constant factors and consolidation of terms, the pertinent equations are

$$1 + R_{TE} = U + D \quad , \tag{66}$$

$$1 - R_{TE} = (k/k_o)(U - D) \quad , \tag{67}$$

$$U\, e^{ikh\cos\theta} + D\, e^{-ikh\cos\theta} = T\, e^{ik_o h\cos\theta} \quad , \tag{68}$$

and

$$\frac{k\cos\theta}{w\mu_o}\left[U\, e^{ikh\cos\theta} - D\, e^{-ikh\cos\theta}\right] = T\,\frac{\cos\theta}{Z_o}\, e^{ik_o h\cos\theta} \quad . \tag{69}$$

2.3.6 SOLUTION OF THE EQUATIONS TO OBTAIN THE TE-REFLECTION COEFFICIENT

Equations (66), (67), (68), and (69) can be solved to obtain R_{TE}, T, U, and D. The solution for the desired TE-reflection coefficient R_{TE} is outlined below. The factor T can be eliminated by combining Eqs. (68) and (69) yielding

$$(k - k_o)\, U = (k + k_o)\, D\, e^{-i2kh\cos\theta} \quad ,$$

or, after rearranging terms,

$$D = U\left(\frac{k - k_o}{k + k_o}\right) e^{i2kh\cos\theta} \quad . \tag{70}$$

Substituting this into Eqs. (66) and (67) and eliminating U gives

$$k(1 + R_{TE})\left[1 - \left(\frac{k - k_o}{k + k_o}\right) e^{i2kh\cos\theta}\right] = k_o(1 - R_{TE}) \left[1 + \left(\frac{k - k_o}{k + k_o}\right) e^{i2kh\cos\theta}\right]$$

which can be solved to find the desired factor

$$R_{TE} = P\,\frac{(1 - e^{i2kh\cos\theta})}{(1 - P^2\, e^{i2kh\cos\theta})} \quad , \tag{71}$$

where

$$P \equiv \left(\frac{k_0 - k}{k_0 + k}\right) = \frac{1 - \sqrt{1 + \dfrac{i\sigma}{w\epsilon_0 \cos^2\theta}}}{1 + \sqrt{1 + \dfrac{i\sigma}{w\epsilon_0 \cos^2\theta}}} \quad . \tag{72}$$

3. GENERAL FEATURES OF THE SLAB TM/TE REFLECTION COEFFICIENTS

3.1 Limiting Forms of the Reflection Coefficients

In order to gain some insights into the nature of the slab reflection processes, it is useful to examine the TM- and TE-slab reflection coefficients for a number of special limiting cases. In doing this it is convenient to consider first the behavior of the propagation constant $\underline{k}$ for three specific limiting cases. This factor is common to both slab reflection coefficients.

From Eq. (22) and the discussion that immediately follows it, the factor $\underline{k}$ can be written as

$$k = k_0 (1 + iG)^{1/2} = A + iB \quad , \tag{73}$$

where

$$G \equiv \sigma/(w\epsilon_0 \cos^2\theta) \quad , \tag{74}$$

and A and B are both positive and real. The following limiting forms can be determined from Eqs. (73) and (74):

(a) For $\sigma \to 0$, or $w \to \infty$

$$k \to k_0 \quad , \tag{75a}$$

(b) For $\sigma \ll 1$, or $w \gg 1$,

$$k \to k_0\left(1 + i\frac{G}{2}\right) \quad . \tag{75b}$$

and

(c) For $\sigma \gg 1$, or $w \ll 1$, $(G \gg 1)$

$$k = k_o(1 + iG)^{1/2} \approx k_o(1 + G^2)^{1/4} e^{i(\tan^{-1} G)/2} \approx k_o G^{1/2}(1 + i1)/2 \quad . \tag{75c}$$

3.1.1 VANISHING CONDUCTIVITY

For the case of vanishingly small σ, or arbitrarily large w, the application of (75a) to Eqs. (38) and (72) shows that both Q and P vanish, respectively, so that

$$\lim_{\substack{\sigma \to 0 \\ \underline{\text{or}}\ w \to \infty}} R_{TM} = 0 \quad , \quad \text{and} \quad \lim_{\substack{\sigma \to 0 \\ \underline{\text{or}}\ w \to \infty}} R_{TE} = 0 \quad .$$

3.1.2 ARBITRARILY LARGE CONDUCTIVITY

For this case, $\sigma \to \infty$ and Eq. (75c) applies. It easily follows that the term $e^{i2h\cos\theta}$ goes to zero. Thus, from inspection of Eqs. (38) and (40), $R_{TM} \to Q \to 1$, and from Eqs. (71) and (72), $R_{TE} \to P \to -1$.

3.1.3 VERTICAL INCIDENCE AND GRAZING INCIDENCE

For vertical incidence, $\theta = 0^o$, and $\cos\theta = 1$, so that it follows from Eqs. (38) and (72) that $P = -Q$, and further, from Eqs. (40) and (71), that $R_{TM} = -R_{TE}$.

For grazing incidence, $\theta \to 90^o$, and $\cos\theta \to 0$. For this case Eq. (75c) is applicable and $e^{i2kh\cos\theta}$ tends to zero. It then follows from inspection of Eqs. (38) and (40) and Eqs. (71) and (72) that $R_{TM} \to -1$, and $R_{TE} \to -1$.

3.1.4 ARBITRARILY LARGE SLAB THICKNESS

It follows from Eq. (73) that as $h \to \infty$, $e^{i2kh\cos\theta}$ becomes vanishingly small. Then, from Eqs. (38) and (40),

$$R_{TM} \to Q = \frac{\left(1 + \dfrac{i\sigma}{w\epsilon_o}\right) - \sqrt{1 + \dfrac{i\sigma}{w\epsilon_o \cos^2\theta}}}{\left(1 + \dfrac{i\sigma}{w\epsilon_o}\right) + \sqrt{1 + \dfrac{i\sigma}{w\epsilon_o \cos^2\theta}}} \quad ,$$

and from Eqs. (71) and (72),

$$R_{TE} \to P \frac{1 - \sqrt{1 + \dfrac{i\sigma}{w\epsilon_0 \cos^2\theta}}}{1 + \sqrt{1 + \dfrac{i\sigma}{w\epsilon_0 \cos^2\theta}}} .$$

It can then be shown, after some rearranging of terms, that these equations are identical to the corresponding classical Fresnel coefficients, such as described by Stratton.[3]

3.1.5 VERY LOW CONDUCTIVITY OR SUFFICIENTLY HIGH FREQUENCY

Under either of these conditions Eq. (75b) applies, and it follows that

$$e^{i2kh\cos\theta} \approx e^{-k_0 Gh\cos\theta}\, e^{i2k_0 h\cos\theta} \approx e^{i2(\frac{w}{c})h\cos\theta} .$$

Then, from Eqs. (40) and (37)

$$R_{TM} \approx Q\left[1 - e^{iw(\frac{2h}{c}\cos\theta)}\right]$$

$$\approx \frac{\sigma(\cos^2\theta - 0.5)}{2\epsilon_0 \cos^2\theta}\left(\frac{1}{-iw}\right)\left[1 - e^{iw(\frac{2h}{c}\cos\theta)}\right] . \qquad (76)$$

Inspection of Eq. (76) shows that the slab TM-reflection coefficient decreases as the incidence angle increases from 0° to 45°, and at 45° it becomes zero. Then as the incidence angle increases, the reflection coefficient increases, with a change in sign, compared to the $\theta < 45^\circ$ case. Thus, it can be concluded that for very weakly conducting slabs, there is a Brewster's angle for an incident TM-wave, which occurs at 45°, regardless of the frequency of the wave.

Similarly, it follows from Eqs. (71) and (72) that for very weakly conducting slabs,

---

3. Stratton, J.A. (1941) Electromagnetic Theory, McGraw-Hill, New York, pp. 492-494.

$$R_{TE} \approx P\left[1 - e^{iw(\frac{2h}{c}\cos\theta)}\right]$$

$$\approx \frac{-\sigma}{4\epsilon_0 \cos^2\theta}\left(\frac{1}{-iw}\right)\left[1 - e^{iw(\frac{2h}{c}\cos\theta)}\right] \quad . \tag{77}$$

Inspection of Eq. (77) shows that the TE-reflection coefficient increases with increasing incidence angle θ, and does not exhibit any Brewster's angle effect.

3.2 Impulse Response of Very Weakly Conducting Slabs

Inspection of Eqs. (76) and (77) shows that functionally the TM- and TE-slab reflection coefficients are identical for the case of very weak conductivity. For this case the slab reflection process can be characterized by considering the factor

$$H(iw) = K\left(\frac{1}{-iw}\right)\left[1 - e^{iw(\frac{2h}{c}\cos\theta)}\right] \quad . \tag{78}$$

In linear systems theory *H(iw) represents the transfer function of the slab,* and its Fourier inverse, h(t), gives the response of the slab to a unit-impulse incident plane wave. Further, H(iw) is functionally equivalent* to the Fourier transform of a time function which is rectangular in shape with amplitude K, and width $T = (2h/c)\cos\theta$, as illustrated in Figure 4. For the case of an infinitely thick slab, the function H(iw) becomes simply (K/-iw), and the impulse response is a step-function of amplitude K, as shown in Figure 4.

It follows from the discussions above that, *more generally*, the impuse response of a very weakly conducting slab is a replica of the slab's conductivity profile. Specifically, the amplitude A of the response at time t relates directly to the conductivity σ of the slab at height z. For the case of vertical incidence, this mapping takes the form (see Eq. (77) for example)

$$[t, A(t)] \rightarrow \left[z = \frac{ct}{2}\ , \quad \sigma(z) \approx 4\epsilon_0 A(t)\right] \quad . \tag{79}$$

This simple mapping is illustrated in Figure 5.

---

*The choice of a spinner e^{iwt} rather than the one used in the derivations in this paper, e^{-iwt}, would have led to an expression for H(iw) that could be directly compared to forms given in most texts on Fourier transforms.

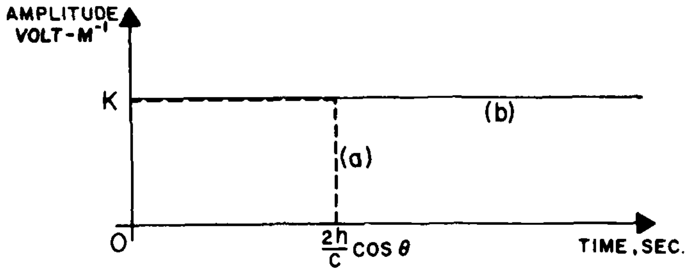

Figure 4. Impulse Responses of Very Weakly Conducting Slabs. (a) Slab with a thickness h, (b) Infinitely thick slab

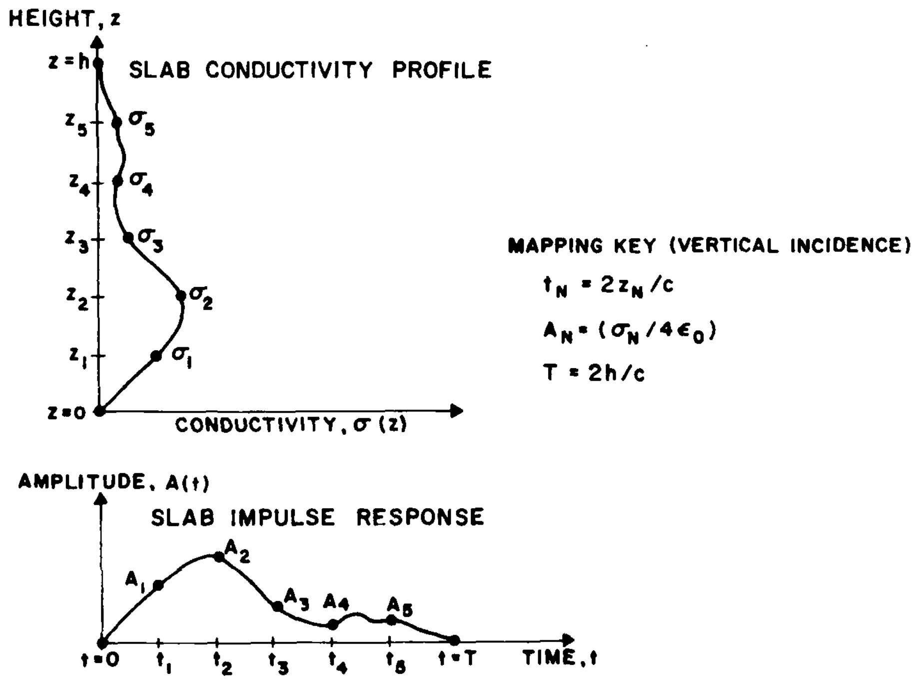

Figure 5. Illustration of the Mapping Between the Conductivity Profile of a Very Weakly Conducting Slab and its Impulse Response

The simple mapping relationships described above are only valid as long as the incident wave penetrates the slab without being significantly altered in any way. This condition breaks down as the conductivity of the slab increases, or as the incidence angle becomes nearly grazing. This will be illustrated by specific numerical examples later in this report.

4. SLAB FREQUENCY RESPONSES

In this section numerical examples are given to illustrate the frequency response characteristics of a few selected conducting slabs. Results are shown for both TM- and TE- incident wave polarizations.

4.1 TM/TE Slab Frequency Responses, Vertical Incidence

As shown by Eqs. (40) and (71), the magnitudes of the TM and TE frequency responses are the same for the case of a vertically incident plane wave. Figure 6 shows the frequency responses calculated for a number of slab thicknesses, with the conductivity held constant, at a value of 2×10^{-9} mho/m. This corresponds to a very weakly conducting case so that the frequency response curve for the example of an infinitely thick slab, in Figure 6, varies as $1/w$ ($w = 2\pi f$), as discussed earlier, with reference to Eqs. (76) and (77). As shown in Figure 6, the response for an infinitely thick slab decreases monotonically with increasing frequency, but for slabs having a finite thickness, the frequency response curves show nulls and relative maxima, which occur in a periodic manner. The frequencies at which the nulls occur can be determined analytically by considering the multiplicative factor $[1 - e^{iw(2h\cos\theta/c)}]$, which occurs in Eqs. (76) and (77). It is a simple matter to show that this factor, and hence the magnitude of the TM/TE reflection coefficient, goes to zero if

$$f = \frac{w}{2\pi} = \frac{Nc}{2h\cos\theta} \quad (N = 1, 2, 3, \ldots) \quad . \tag{80}$$

Thus, for the h = 3 km example shown in Figure 6, the nulls occur at multiples of 50 kHz, while for the h = 7.5 km example, they occur at multiples of 20 kHz, etc.

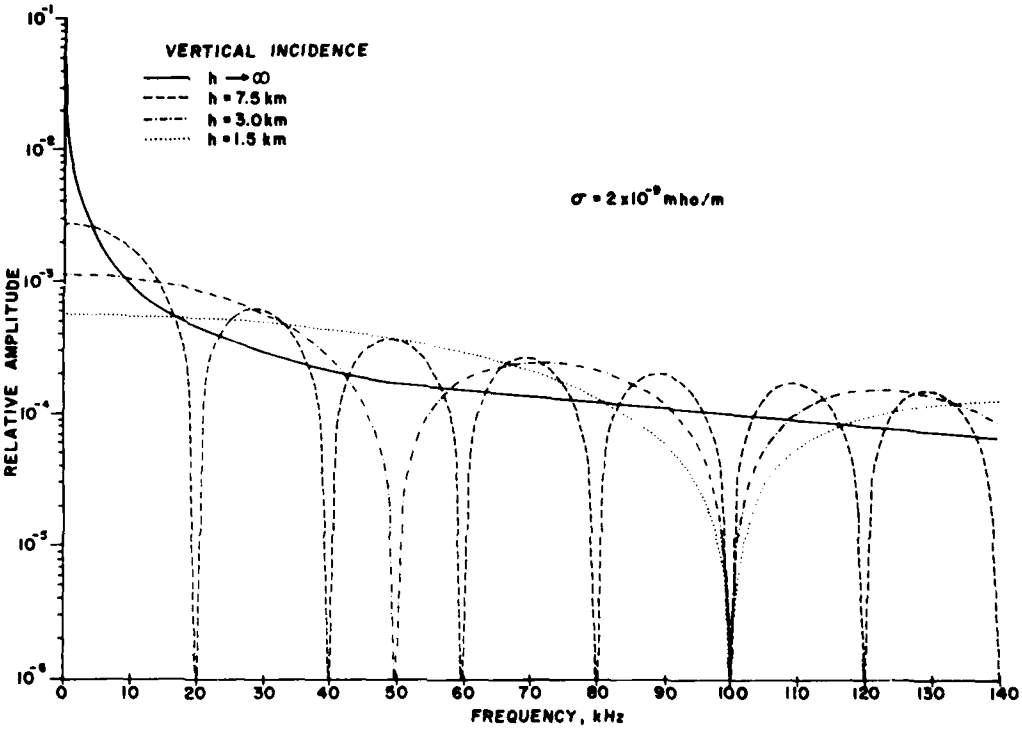

Figure 6. Dependence of TM/TE Frequency Responses on Slab Thickness; Vertical Incidence, $\sigma = 2 \times 10^{-9}$ mho/m

4.2 Slab Frequency Response as a Function of Incidence Angle

4.2.1 TM-POLARIZATION

Figure 7 shows the TM frequency response of a weakly conducting slab for a number of incidence angles. In all cases the slab was assumed to be 7.5 km thick, with a conductivity of 2×10^{-9} mho/m. Inspection of the curves in Figure 7 and the h = 7.5 km curve in Figure 6 shows that for a fixed frequency, the slab reflectivity generally decreases as the incidence angle varies from 0° (vertical incidence) to 45°, at which point the slab exhibits a Brewster's angle effect. Then, as the incidence angle increases above 45°, the slab becomes a better reflector, and the amplitudes of the reflected waves become larger, as shown in Figure 7. As discussed earlier, the slab becomes an almost perfect reflector at extremely grazing incidence angles ($\theta \rightarrow 90^{\circ}$).

Figure 7 also shows that the location of the relative nulls in the slab's frequency response changes as the incidence angle varies. Further, as the incidence angle increases, the spacing between the nulls also increases. Inspection of the

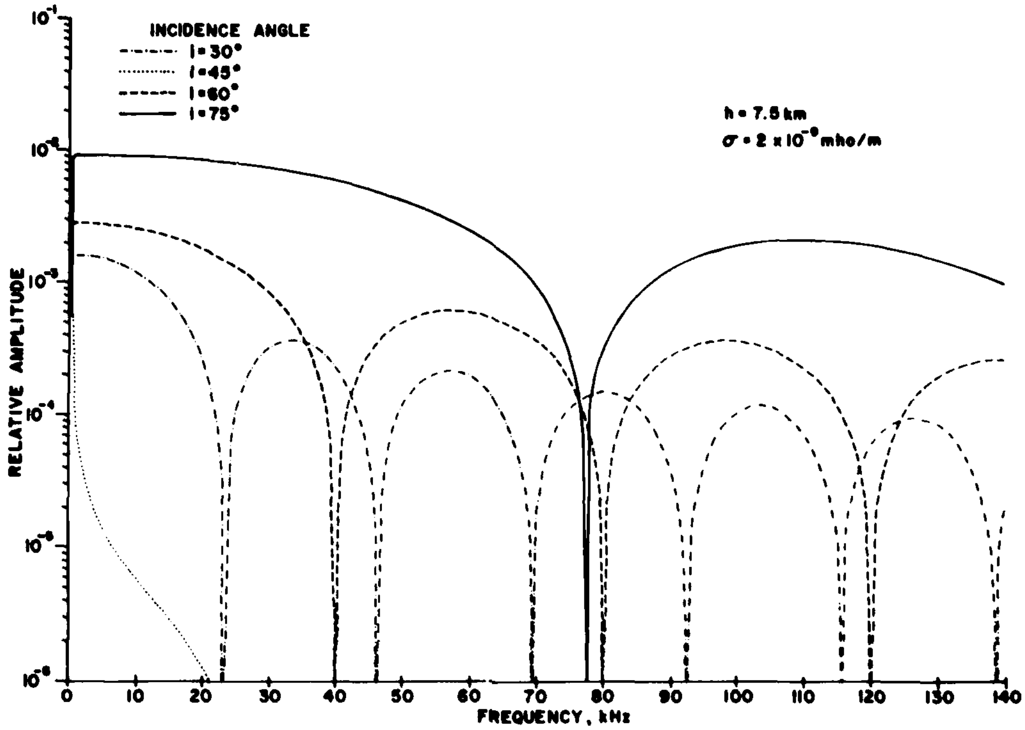

Figure 7. TM Slab Frequency Responses for a Number of Incidence Angles; h = 7.5 km, and $\sigma = 2 \times 10^{-9}$ mho/m

curves in Figure 7 show that the null spacings are inversely proportional to $\cos\theta$, and follow the relationship given by Eq. (80) earlier.

4.2.2 TE-POLARIZATION

Calculations of TE-frequency response curves for two incidence angles are shown in Figure 8, for the same 7.5 km thick slab which has been described above. These curves, along with others not shown here, show that for a given frequency, the slab's TE-reflectivity increases as the incidence angle varies from 0° to 90°. No Brewster's angle occurs, and in general, for the same frequency and incidence angle, the TE reflection amplitude is greater than the TM-reflection amplitude. The TE-frequency response curves exhibit the same null patterns as discussed for the TM-case, with the null pattern again following the form given by Eq. (80).

Examination of Eq. (80), which shows how the null patterns vary with incidence angle and/or slab thickness, illustrates that for a fixed incidence angle, the null spacing will increase with decreasing slab thickness (see for example,

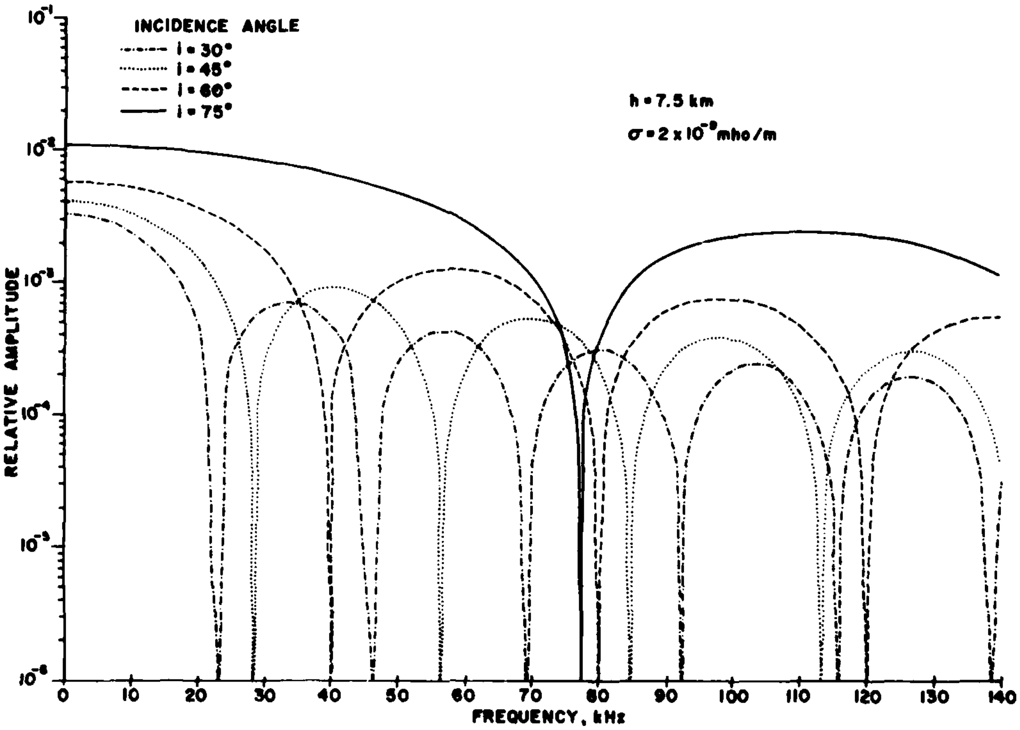

Figure 8. TE Slab Frequency Responses; h = 7.5 km, and σ = 2×10^{-9} mho/m

Figure 6). Alternately, for a fixed slab thickness, the null spacing will increase with increasing incidence angle. In a sense then, as the incidence angle increases, the "apparent" thickness of the slab decreases. This aspect of plane-wave slab reflectivity will be discussed in more detail in a later section of this report.

5. SLAB IMPULSE RESPONSES

The reflection properties of conducting slabs are characterized by the reflection coefficients given in Eqs. (40) and (71). Following well known Fourier transform approaches, these expressions can be used to determine the responses of the slab to an aggregate of incident plane waves whose sum represents a unit-impulse. The resulting impulse-response can then be convoluted with any arbitrary incident waveform to obtain the resultant slab reflected waveform. In this section slab impulse responses are shown for a variety of slab conductivities, thicknesses, and incidence angles. The results were obtained by use of digital

integrations of the expressions for the impulse responses. In general, since the responses must be purely real, and identically equal to zero for $t < 0$, the impulse responses can be written, following the e^{-iwt} spinner adopted in this report, as

$$\delta(t) = \frac{1}{2\pi} \int_{-\infty}^{\infty} R(iw)\, e^{-iwt}\, dt = \frac{1}{\pi} \operatorname{Re} \int_{0}^{\infty} R(iw)\, e^{-iwt}\, dt = \frac{1}{\pi} \operatorname{Re} \int_{0}^{\infty} R(w)\, e^{i\phi(w)}$$

$$e^{-iwt}\, dw$$

where $R(w)$ and $\phi(w)$ are the magnitude and phase of the slab reflection coefficient, determined from either Eq. (40) or (71), depending on the polarization of the incident waves. This can further be reduced to the relatively simple form

$$\delta(t) = \frac{1}{\pi} \int_{0}^{\infty} R(w) \cos\left[wt - \phi(w)\right] dw \quad , \qquad (81)$$

which can be numerically integrated, using well established digital techniques.

5.1 Slab TM-Impulse Responses

5.1.1 VERY WEAKLY CONDUCTING SLAB, VERTICAL INCIDENCE

Figure 9 shows the impulse responses of a slab with conductivity 2×10^{-9} mho/m, for three slab thicknesses, $h = 1.5$ km, $h = 7.5$ km, and $h \to \infty$. For the infinitely thick case, the impulse response is essentially a step-function with an amplitude of approximately 56.5, while for the cases of finite slab thickness, the impulse responses are rectangular in shape, having the same amplitude of 56.5, but different widths. For the 7.5 km example, the pulse-width is 50 μsec, while for the 1.5 km example, it is only 10 μsec. These results are in agreement with those expected for very weakly conducting slabs, as discussed earlier in Section 3.2 of this report, and the amplitude and pulse widths shown in Figure 9 follow the mapping relationship given in Eq. (79).

5.1.2 VERY WEAKLY CONDUCTING SLAB, VARYING INCIDENCE ANGLE

Figure 10 summarizes the impulse responses of a very weakly conducting slab ($\sigma = 2 \times 10^{-9}$ mho/m) under a variety of conditions. In all cases the impulse responses are rectangular in shape with amplitudes and widths which vary with

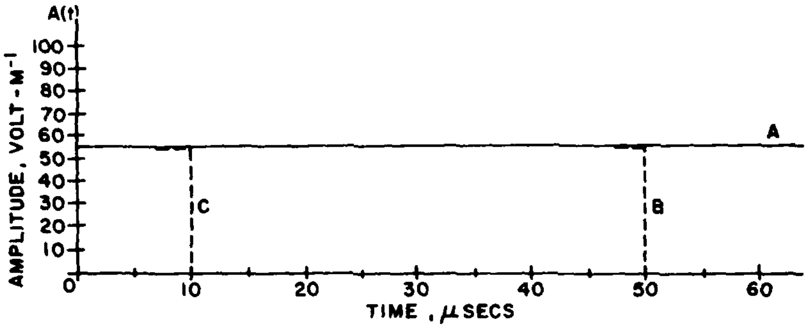

Figure 9. Impulse Responses of a Very Weakly Conducting Slab; $\sigma = 2 \times 10^{-9}$ mho/m. (a) Infinitely thick slab, (b) 7.5 km thick slab, (c) 1.5 km thick slab

assumed incidence angle and slab thickness. Figure 10(a) shows that for a fixed incidence angle ($\theta = 0^{\circ}$), the width of the impulse response varies linearly with slab thickness. Figure 10(b) shows the variation of the duration of the impulse response with incidence angle, for a 7.5 km thick slab. The duration of the impulse response is maximum for the case of vertical incidence ($\theta = 0^{\circ}$), and approaches zero as the incidence angle tends to 90°. The variation of the magnitudes of the impulse responses with incidence angle is shown in Figure 10(c), for a 7.5 km thick slab. As the incidence angle increases the amplitudes at first decrease, but then increase, with a change of sign. The changeover in the amplitude effect occurs at an incidence angle of 45°, which is the slab's Brewster angle. At that angle, the slab's impulse response is negligibly small. In summary, the amplitudes of the impulse responses follow the form $\sigma(2\cos^2\theta - 1)/(4\epsilon_0 \cos^2\theta)$, and the widths follow the form $(2h/c)\cos\theta$, which are in accordance with the results expected for a very weakly conducting slab, as discussed earlier in Section 3.2 of this report.

The decreases in response times that are seen in Figure 10(b) as the incidence angle is changed, are similar to those that occur when the thickness of the slab is decreased, while the incidence angle is fixed. In effect then, Figure 10(b) illustrates that the "apparent" thickness of the slab is reduced as the incidence angle increases. In the limit, as the incidence angle becomes almost grazing, the "apparent" slab thickness approaches zero. This result suggests that for any incident waveform described by plane waves, the geometry of the slab reflection process itself will cause the reflected waveform to be extended in time by an amount ΔT that will be related to the incidence angle. For vertical incidence, ΔT will be a maximum, while for very nearly grazing angles, it will be practically zero. The geometry which illustrates that is shown in Figure 11.

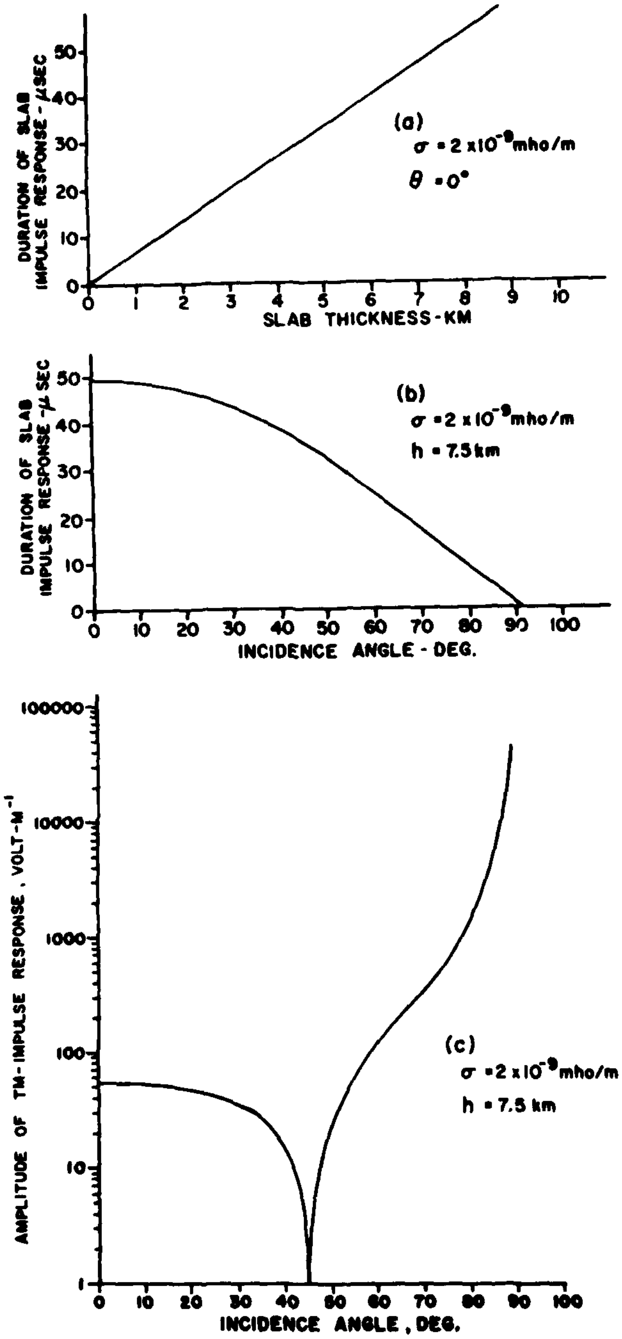

Figure 10. TM Impulse Response Characteristics for a Very Weakly Conducting Slab; $\sigma = 2 \times 10^{-9}$ mho/m. (a) Duration of impulse response as a function of slab thickness, (b) duration of slab impulse response as a function of incidence angle, h = 7.5 km, (c) amplitude of TM-impulse response as a function of incidence angle, h = 7.5 km

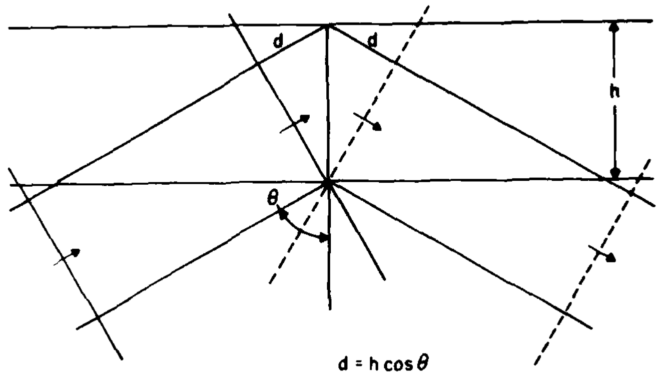

Figure 11. Geometry Illustrating the Plane Wave Difference in Path Length to an Observer for Reflections from Two Levels in a Slab which are Separated by a Distance h

The construction shown in Figure 11 shows that an observer in the space below the slab would sense the reflected energy from a level h above the bottom of the slab, at a time ΔT later than that reflected from the bottom of the slab. The time ΔT is simply related to the distance 2d shown in the figure, and can be expressed as $\Delta T = (2h/c) \cos \theta$.

5.1.3 VERTICAL INCIDENCE, VARYING CONDUCTIVITY AND SLAB THICKNESS

Figure 12 shows slab impulses for a wide range of conductivities and slab thicknesses. In all cases, vertical incidence is assumed. In Figure 12(a) the assumed conductivity is 2×10^{-9} mho/m, and the curves include those already discussed with reference to Figure 9. As noted earlier, for this very weakly conducting slab example, the impulse responses are replicas of the slab conductivity profiles, with the mapping from one to the other given by Eq. (79).

Figure 12(b) shows the impulse responses for an assumed conductivity of 2×10^{-7} mho/m. In this case, the response for an infinitely thick slab no longer is a step-function, but rather, drops off gradually with increasing time. Although the approximations and mapping relationships which were developed for very weakly conducting slabs do not apply for this case, the effects of changing the thickness of the slab are still very noticeable in the way in which the responses drop off. For example, for the 1.5 and 7.5 km examples, the responses drop off almost instantaneously at times given by 2h/c. As the slab thickness increases however, the drop-offs become more gradual and sluggish until, for very large thicknesses (for example, h = 90 km), the responses cannot be distinguished very well from the response of the infinitely thick slab.

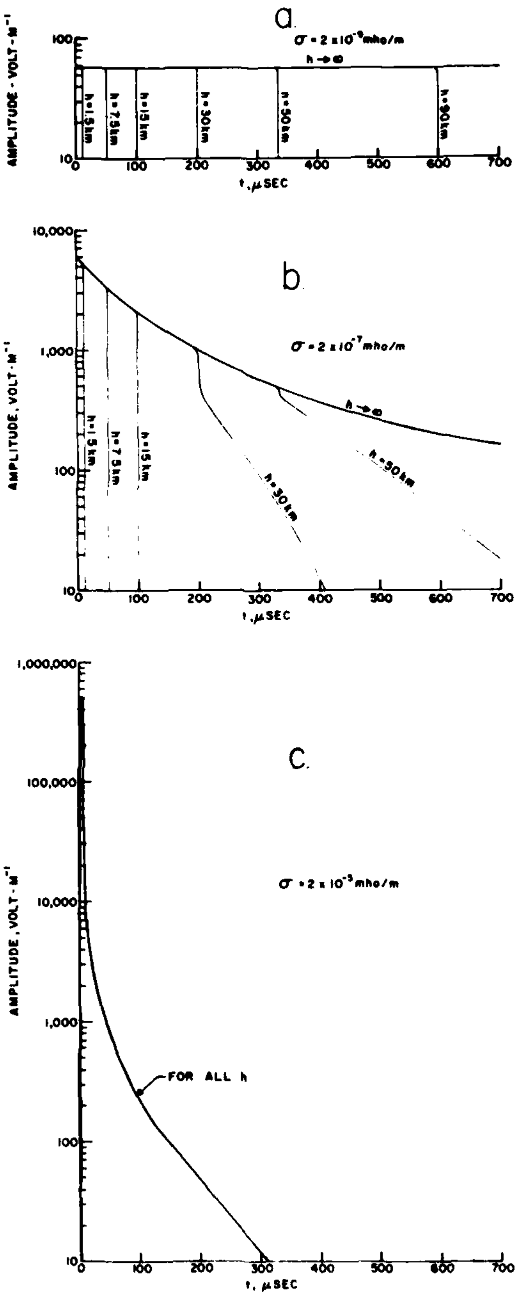

Figure 12. Slab TM Impulse Responses as a Function of Slab Thickness and Conductivity. (a) $\sigma = 2 \times 10^{-9}$ mho/m, (b) $\sigma = 2 \times 10^{-7}$ mho/m, (c) $\sigma = 2 \times 10^{-5}$ mho/m

Figure 12(c) shows corresponding impulse responses for an assumed conductivity of 2×10^{-5} mho/m. For an infinitely thick slab, the response is impulsive, *rising very sharply* and then rapidly dropping off. In the example shown in Figure 12(c), the impulse responses for the various slab thicknesses assumed cannot be distinguished from the infinitely thick case. This indicates that because of the relatively high conductivity assumed, the reflection process is very nearly a Fresnel-like sharp boundary one.

5.2 Slab TE-Impulse Responses

TE-impulse response studies were conducted similar to those described with reference to Figures 10 to 12. The results of one such study are shown in Figure 13, where TE-impulse responses are given over a wide range of incidence angles, for the case of a 7.5 km thick slab having a conductivity of 2×10^{-9} mho/m. Comparisons of the results for this very weakly conducting slab case with those of

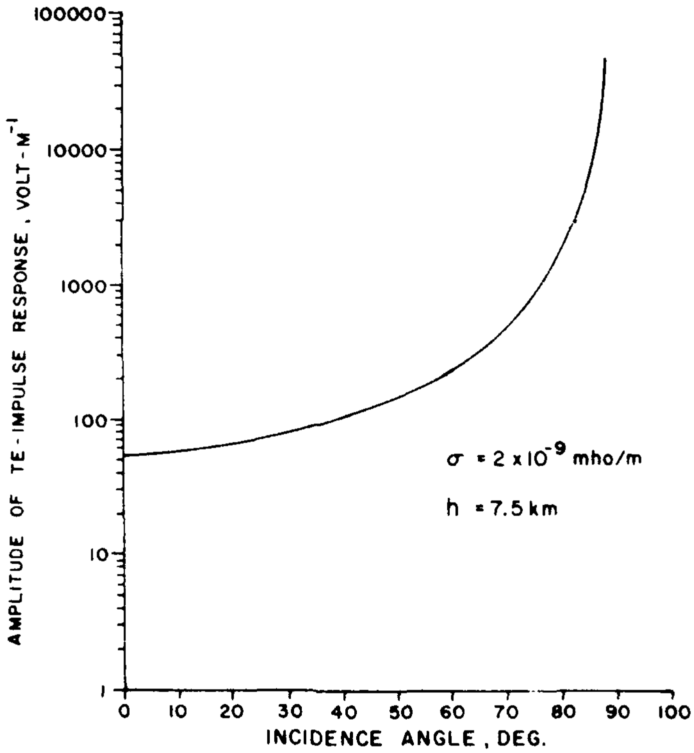

Figure 13. Slab TE Impulse Responses as a Function of Incidence Angle; h = 7.5 km, and $\sigma = 2 \times 10^{-9}$ mho/m

Figure 10(c) show that there are no Brewster's angle effects associated with the TE-responses, and that the TE-amplitudes are larger than the corresponding TM-amplitudes. It follows from Eqs. (76) and (77) that for very weakly conducting slabs, the TM to TE amplitude ratio can be expressed simply as $(1 - 2\cos\theta)$. This shows that the two amplitudes are of opposite sign for incidence angles less than 45°. The TM Brewster's angle is at 45°, and for incidence angles greater than 45°, the two responses have the same sign. The relationship also shows that the two amplitudes are equal only for incidence angles of zero or 90°.

The results of other TE-impulse response studies, not shown here, were very similar to those already discussed in conjunction with the TM-examples of Figures 10(a, b) and 12.

6. SLAB REFLECTION OF PULSES

Using well established Fourier transform methods, it is a relatively simple matter to determine the waveforms of pulses that have been reflected from conducting slabs. Specifically, if the Fourier transform of the incident pulse is $C(iw)$, and the transfer function of the slab is defined by $R(iw)$, then the reflected pulse $v(t)$ can be found from the Fourier inverse $F^{-1}[C(iw)R(iw)]$. For purely real functions, defined for $t \geq 0$, it follows that in the notations adopted earlier in this report

$$V(t) = \frac{1}{\pi} \operatorname{Re} \int_0^{\infty} C(iw)R(iw)\, e^{-iwt}\, dw \quad ,$$

$$= \frac{1}{\pi} \int_0^{\infty} CR \cos(wt - \psi)\, dw \quad , \tag{82}$$

where

$$C(iw) \equiv C\, e^{i\alpha} \quad ,$$

$$R(iw) \equiv R\, e^{i\phi} \quad ,$$

and

$$\psi = \alpha + \phi \quad .$$

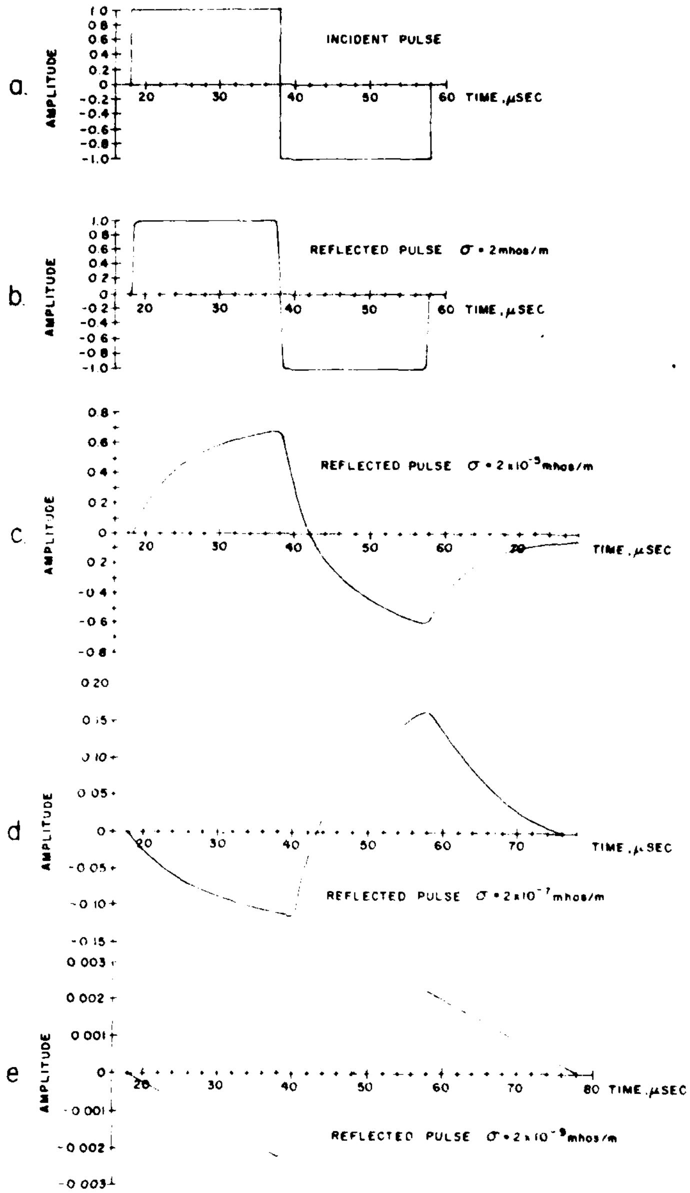

Figure 14. Slab TM Reflections of Single-Cycle Square-Wave Pulses. (a) Incident pulses, (b) reflected pulses, $\sigma = 2$ mho/m, (c) reflected pulse, $\sigma = 2 \times 10^{-5}$ mho/m, (d) reflected pulse, $\sigma = 2 \times 10^{-7}$ mho/m, (e) reflected pulse, $\sigma = 2 \times 10^{-9}$ mho/m. In all cases the incidence angle is 60° and the slab thickness is 6 km

Figure 14 illustrates the results of the application of Eq. (82) to determine TM-pulse reflections from a 6 km thick slab. In the examples shown, the incident pulse was a single-cycle square-wave of unit amplitude, as shown in Figure 14(a), and the incidence angle was 60°. In Eq. (82), R(iw) is given by Eq. (40) and

$$C(iw) = \left(\frac{1}{-iw}\right)\left[e^{i(0.000018w)} - 2\,e^{i(0.000038w)} + e^{i(0.000058w)}\right] .$$

For a conductivity of 2 mho/m the reflected pulse, shown in Figure 14(b) is practically identical to the incident pulse, but for the much weaker conductivity example shown in Figure 14(c), for which $\sigma = 2 \times 10^{-5}$ mho/m, the reflected pulse is significantly altered, both in amplitude and in pulse width. Figure 14(d) shows that for a conductivity of 2×10^{-7} mho/m, the polarity of the reflected pulse is opposite to that of the incident pulse, indicating that the 60° incidence angle is beyond the Brewster's angle of the slab. For a very weakly conducting slab, $\sigma = 2 \times 10^{-9}$ mho/m, the reflected pulse is directly proportional to the integral of the incident pulse, as shown in Figure 14(e). This is in accordance with Eq. (78). Further, for this example the incidence angle is beyond the slab's Brewster's angle of 45°, and the reflected pulse is 20 μsec longer than the incident pulse, as expected from the $\Delta T = (2h/c) \cos \theta$ relationship discussed earlier in Section 5.

7. DISCUSSION

Equations (40) and (71) can be used to predict the reflection coefficients and impulse responses of conducting slabs; and, in conjunction with Fourier transform methods, they also provide the means for computing the waveform of a slab-reflected pulse if the waveform of the incident pulse is specified. In experimental programs, however, questions naturally arise as to what polarization, wave frequencies, and incidence angles should be used for remote sensing or "sounding" of a slab's thickness and conductivity.

The optimum polarization for sounding purposes is the Transverse Electric (TE), because TE-waves reflect more strongly than Transverse Magnetic (TM) waves from conducting slabs. Also, the TE-polarization is free of Brewster's angle effects, which can make the interpretation of TM reflection data more complex and ambiguous.

Vertical or nearly vertical incidence angles are preferred over very oblique (grazing) ones. For example, TM reflection amplitudes decrease with increasing

incidence angle until the Brewster's angle is reached, and, except for grazing angles, they are largest at vertical incidence. Conversely, TE reflection amplitudes increase with increasing incidence angle, so that there may be practical advantages to TE-sounding at oblique angles, but grazing angles should be avoided. At such angles the slab reflection process approaches that of a sharp boundary (for both TM and TE waves), resulting in a loss of information on the thickness of the conducting slab.

The preferred frequencies for sounding with pulses are intimately linked to the conductivity of the slab and the incidence angle which is used. However, as described earlier, if the inequality (Eq. (75b)) is satisfied, the determination of a slab's thickness and conductivity from observations of its pulse reflections becomes particularly simple. Specifically, Eq. (78) holds so that the incident pulse becomes integrated upon reflection, and has amplitudes that are directly proportional to the conductivity of the slab. Furthermore, the dispersion of the incident pulse, upon reflection, is directly proportional to the thickness of the slab, as described earlier in conjunction with Figure 14(e).

Inequality Eq. (75b) can be rewritten as

$$f_{kHz} \gg \frac{1.8 \times 10^7}{\cos^2 \theta} \sigma \quad . \tag{83}$$

Thus, for example, for a conductivity of 2×10^{-7} mho/m and vertical incidence, the preferred sounding frequencies would satisfy $f_{kHz} \gg 3.6 \approx 360$ kHz, while for a conductivity of 2×10^{-9} mho/m, the preferred frequencies would be greater than only 3.6 kHz. For an incidence angle of 60^0 however, the preferred frequencies are greater than 1.44 MHz and 14.4 kHz, respectively, for these examples. Figure 15 summaries the application of inequality Eq. (83) for estimating preferred sounding frequencies.

In some instances the "preferred" sounding frequencies determined from inequality Eq. (83) may not be practical from an experimental point of view. For example, the authors have conducted studies of the C-layer of the lower daytime lower ionosphere which has conductivities in the order of 2×10^{-7} mho/m.[1] The preferred sounding frequencies for such a conductivity would be in the 360 kHz range or greater, but at such high frequencies the amplitudes of the reflections would be too low to be measured, particularly in the presence of noise. Using pulse sounding in the 10 to 50 kHz range, however, in conjunction with digital processing, it was possible to deduce that the thickness of the C-layer being observed was about 6 km. This was done by use of an iterative technique involving Eqs. (82) and (40). It has been the authors' experience that good estimates of slab conductivity and thickness can be achieved within a few iterations via this technique.

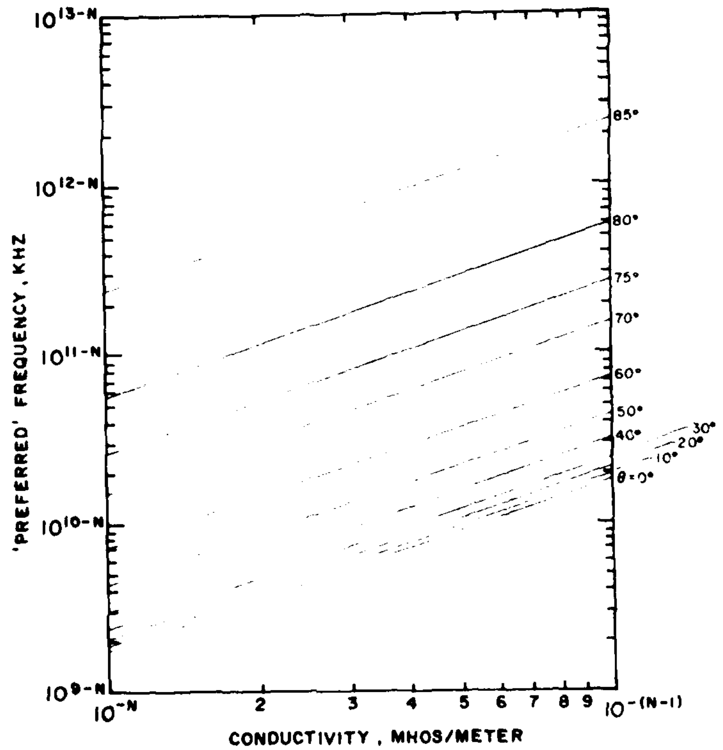

Figure 15. Preferred Sounding Frequencies as a Function of Slab Conductivity and Incidence Angle

MISSION
of
Rome Air Development Center

RADC plans and executes research, development, test and selected acquisition programs in support of Command, Control Communications and Intelligence (C^3I) activities. Technical and engineering support within areas of technical competence is provided to ESD Program Offices (POs) and other ESD elements. The principal technical mission areas are communications, electromagnetic guidance and control, surveillance of ground and aerospace objects, intelligence data collection and handling, information system technology, ionospheric propagation, solid state sciences, microwave physics and electronic reliability, maintainability and compatibility.

EN

DAT

FILME

6 - 8

DTI